Title	Photoacoustic microscopy imaging for microneedle drug delivery
Author(s)	Moothanchery, Mohesh; Seeni, Razina Z.; Xu, Chenjie; Pramanik, Manojit
Citation	Moothanchery, M., Seeni, R. Z., Xu, C., & Pramanik, M. (2018). Photoacoustic microscopy imaging for microneedle drug delivery. Proceedings of SPIE - Photons Plus Ultrasound: Imaging and Sensing 2018, 10494, 104945P-.
Date	2018
URL	http://hdl.handle.net/10220/44470
Rights	

Photoacoustic microscopy imaging for microneedle drug delivery

Mohesh Moothanchery, Razina Z. Seeni, Chenjie Xu, Manojit Pramanik*

School of Chemical and Biomedical Engineering, Nanyang Technological University, Singapore

ABSTRACT

The recent development of novel transdermal drug delivery systems (TDDS) using microneedle technology allows micron-sized conduits to be formed within the outermost skin layers attracting keen interest in skin as an interface for localized and systemic delivery of therapeutics. In light of this, researchers are using microneedles as tools to deliver nanoparticle formulations to targeted sites for effective therapy. However, in such studies the use of traditional histological methods are employed for characterization and do not allow for the *in vivo* visualization of drug delivery mechanism. Hence, this study presents a novel imaging technology to characterize microneedle based nanoparticle delivery systems using optical resolution-photoacoustic microscopy (OR-PAM). In this study *in vivo* transdermal delivery of gold nanoparticles using microneedles in mice ear and the spatial distribution of the nanoparticles in the tissue was successfully illustrated. Characterization of parameters that are relevant in drug delivery studies such as penetration depth, efficiency of delivered gold nanoparticles were monitored using the system. Photoacoustic microscopy proves an ideal tool for the characterization studies of microneedle properties and the studies shows microneedles as an ideal tool for precise and controlled drug delivery.

Keywords: Microneedles, Transdermal delivery, Optical resolution photoacoustic microscopy, PAM, OR-PAM, Photoacoustic imaging

1. Introduction

Microneedles are emerging transdermal drug delivery tool offering pain free, bio safe, patient friendly, drug release control and easy termination of therapy [1-3]. This technology creates micropores in the stratum corneum, and enables the delivery of a broad range of therapeutics that cannot permeate intact skin [4]. Compared to solid microneedles made of metal, ceramics and silicon, polymeric microneedles gained extensive attention over the years due to their nontoxicity, biodegradability, biocompatibility and easy fabrication [5, 6]. Cancer is one of the leading causes of death worldwide [7]. Photodynamic therapy (PDT) has emerged as one of the important therapeutic selections for treatment of cancer and other diseases [8]. Penetration and accumulation of cancer therapeutics to the hypoxic center of the tumor is often limited due to the large intercapillary distances and variable blood flow of solid tumors [9, 10]. The outer shell of solid tumors is often the site of angiogenesis. This highly vascularized angiogenic blood vessels have gaps up to 600 nm between adjacent endothelial cells, allowing carriers to extravasate into the interstitial space [11]. It was showed that Gold nanoparticles (GNPs) can enhance singlet oxygen generation or photodynamic therapy efficiency of different photosensitizers [12, 13]. GNPs themselves could be used as therapeutic agents to destroy tumor cells, and also can be used to trigger drug release [14, 15]. Therapeutics are normally delivered intravenously which elicit toxicity to normal cells and cause severe side effects. Therefore new and improved target specified therapeutic delivery is needed. Previous studies shows the potential of MNs in enhancing delivery of photosensitising agents for photodynamic therapy [16]. Delivering photosensitising drugs using this platform has been demonstrated to have several advantages over conventional photodynamic therapy. One common method in designing nanoparticles for passive uptake takes advantage of the hyperpermeability of solid tumor. It is important to visualize and characterize the MNs' properties including penetration depth, dissolution in skin as well as drug release profiles. Mainly *ex vivo* techniques such as biopsy and histological staining was

* E-mail: manojit@ntu.edu.sg

Photons Plus Ultrasound: Imaging and Sensing 2018, edited by Alexander A. Oraevsky, Lihong V. Wang, Proc. of SPIE Vol. 10494, 104945P · © 2018 SPIE · CCC code: 0277-786X/18/$18 · doi: 10.1117/12.2287837

employed [17] which are time-consuming and require the excision and processing of tissue specimens. In addition, the results derived with those destructive methods are often inaccurate as skin tissue is elastic and usually do not retain the microstructure generated during MNs insertion. Therefore, imaging technologies that provide real-time non-invasive *in vivo* images of the MNs' penetration and drug delivery in skin are highly desired. Researchers employed optical coherence tomography to study MNs behaviours in transdermal drug delivery [18-20]. OCT have limited contrast and have difficulty in differentiating between the MNs and the skin layers [18, 20].

It is challenging to maintain both superb spatial resolution and deep penetration depth for pure optical imaging techniques like confocal microscopy, multiphoton microscopy and optical coherence tomography (OCT) [21-23]. Photoacoustic Microscopy (PAM) is a fast-growing hybrid *in vivo* imaging modality combining optical contrast with ultrasound resolution which overcomes the limitations of other existing optical modalities [24-28]. PAM can provide penetration beyond optical mean free path (~1 mm in skin) with high resolution and has been successfully applied to *in vivo* structural, functional, molecular, and cell. In PAM a short laser pulse irradiates the tissue/sample. There will be a temperature rise due to absorption of light by the tissue chromophores (such as melanin, red blood cells, water etc.), which in turn produces pressure waves as acoustics waves. A wideband ultrasonic transducer receives the acoustic signal outside the tissue/sample boundary. Here we conducted detailed characterization studies regarding penetration depth, drug delivery using coated microneedles. Studies on the penetration of microneedles for effective drug delivery at different depths were studied using OR-PAM.

2. Experimental set up

The schematic of the OR-PAM system is shown in Fig. 1 and explained in detail [29]. The laser beam from a nanosecond tunable laser system was reshaped by an iris and spatially filtered by a condenser lens, CL and pinhole, PH arrangement. The beam was attenuated by a neutral density filter, NDF and coupled to a single-mode fiber, SMF. The output beam from the SMF was collimated by an Achromatic lens, L1 and filled the entire back aperture of another identical Achromatic lens, L2. The focusing beam will be passed through a optoacoustic beam combiner consisting of a right angled prism, RA and a rhomboid prism, RP with a layer of silicon oil, SO in between. The silicon oil layer acts as optically transparent and acoustically reflective film. An acoustic lens, AL provided acoustic focusing (focal diameter ~46 μm) was attached at the bottom of the rhomboid prism. The ultrasonic transducer, UST having center frequency 50 MHz was placed on top of the rhomboid. The laser repetition rate for the OR-PAM was set to 5 kHz and the laser energy at focus can be varied up to 200 nJ per pulse.

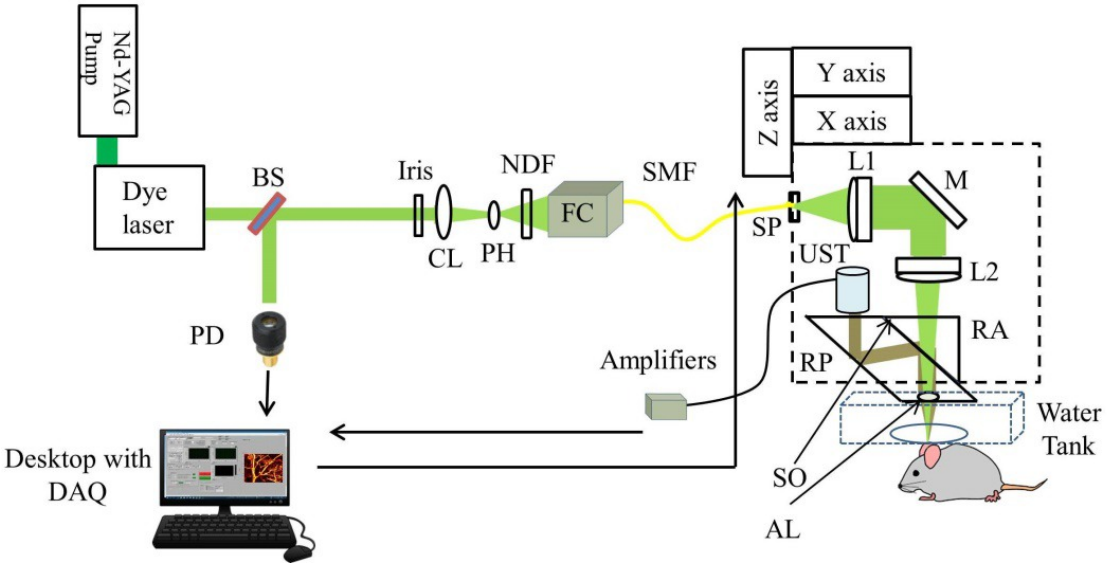

Fig.1. Schematic of the OR-PAM imaging system. BS - Beam Sampler, NDF - Neutral density filter, PD - photodiode, CL - Condenser lens, PH - Pinhole, FC - Fiber coupler, SMF - Single mode fiber, SP - Slip plate, DAQ - Data acquisition card, L1&L2 - Achromatic doublet, M - Mirror, RA - Right angle prism, RP - Rhomboid prism, UST - Ultrasound transducer, AL - Acoustic lens, SO - Silicon oil.

The OR-PAM scan head was attached to a 3-axis motorized stage. The bottom of the OR-PAM scanner head was submerged in a water-filled tank during photoacoustic imaging. An imaging window was opened in the bottom of the tank and sealed with a polyethylene membrane for optical and acoustic transmission. The PA signal acquired by the UST was amplified by two amplifiers having 24 dB gain, and was recorded using a data acquisition card, DAQ in a desktop computer. The scanning and data acquisition was controlled using Labview software. Two-dimensional continuous raster scanning of the imaging head was used during image acquisition. The synchronization of the data acquisition and the stage motion was controlled through the signal from a photodiode, PD. A beam sampler, BS was placed in front of the laser beam diverted a small portion of the beam (5%) to the PD. The PD signal was also used for compensating pulse to pulse variations during data acquisition. All experiments were done at a laser wavelength of 570 nm. The use of photopolymer material [30, 31] for making a transparent casing and using MEMS scanner [32, 33] can improve the footprint of the system for clinical applications.

3. Results and discussion

3.1 Fabrication and Characterization of the MNs patch

The poly(methyl methacrylate) (PMMA) MNs were designed by Micropoint Technologies Pte Ltd (Singapore) in a 10×10 array having a base width of 300 μm and height of 600 μm. Safety and high mechanical toughness to withstand MNs compression when inserted into skin makes PMMA an ideal candidate for MNs manufacturing.

AuNPs of size 100 nm was coated to PMMA MNs. The surface of the MNs was cleaned with acetone and blown dry with nitrogen gas. The MNs surface was then plasma treated using Harrick Plasma Cleaner PDC 32G. The MNs were dipped into 0.1 ml of concentrated AuNPs solution for several times ensuring that the solution covered the surface of the MNs and was dried in the oven at 80° C overnight.

Photograph of PMMA microneedles array used for our studies were shown in Fig. 2(a). Figures 2(b) and 2(c) show the optical microscope image of the microneedles. From Fig. 2(c) we can confirmt he base width and height of the needles.

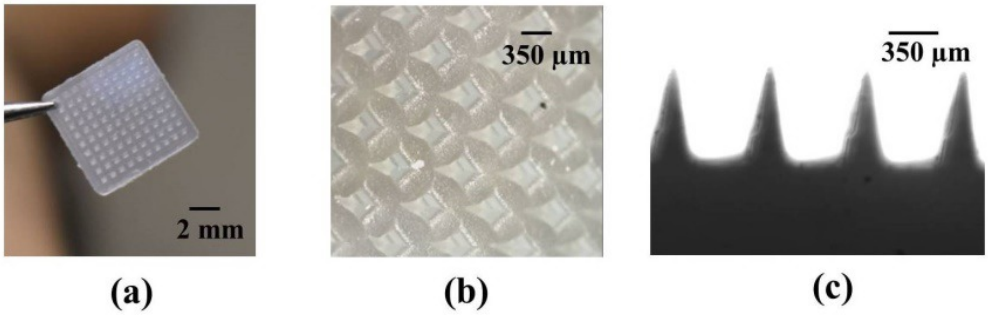

Fig 2. (a) PMMA Microneedles (b) and (c) Optical Microscope image of the needle.

3.2 Photoacoustic imaging of the skin penetration of MNs

In order to monitor the MNs' real-time characteristics and penetration of nanoparticles in biological tissues non-invasively, we used OR-PAM system. The ear of a female mice of body weight 25 g and age 4 weeks, procured from InVivos Pte. Ltd. Singapore, were used in the imaging experiments. Animal experiments were performed according to the approved guidelines and regulations by the institutional Animal Care and Use committee of Nanyang Technological University, Singapore (Animal Protocol Number ARF-SBS/NIE-A0263). The animals were

anesthetized using a cocktail of Ketamine (120 mg/kg) and Xylazine (16 mg/kg) injected intraperitoneally (dosage of 0.1 ml/10 gm). After removing hair from the ear the mouse was positioned on a microscopic glass slide before the MNs coated with AuNPs was pressed into a mouse ear using an applicator. MNs were placed in mouse ear for 60 seconds and OR-PAM imaging was performed. The animal was further anesthetized with vapourised isoflurane system (1 L/min oxygen and 0.75% isoflurane) during the imaging period. A 3 mm × 1.5 mm area of the mouse ear was imaged using OR-PAM after microneedle insertion with a step size of 2 µm along X-axis and 4 µm long Y-axis. The Maximum Amplitude Projection (MAP) images is shown in Fig. 3.

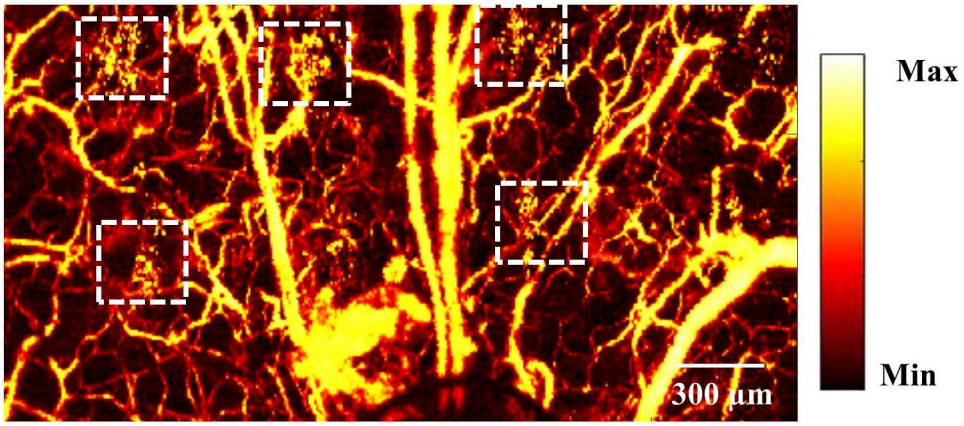

Fig 3**.** *In vivo* photoacoustic image of mouse ear after MNs insertion.

In order to characterize the penetration depth efficiency of nanoparticles delivery at each depth MAP images were reconstructed at different depth. Figures 4 (a)-(d) show the MAP images of Fig. 3(c) at different depth from surface of skin after MNs insertion.

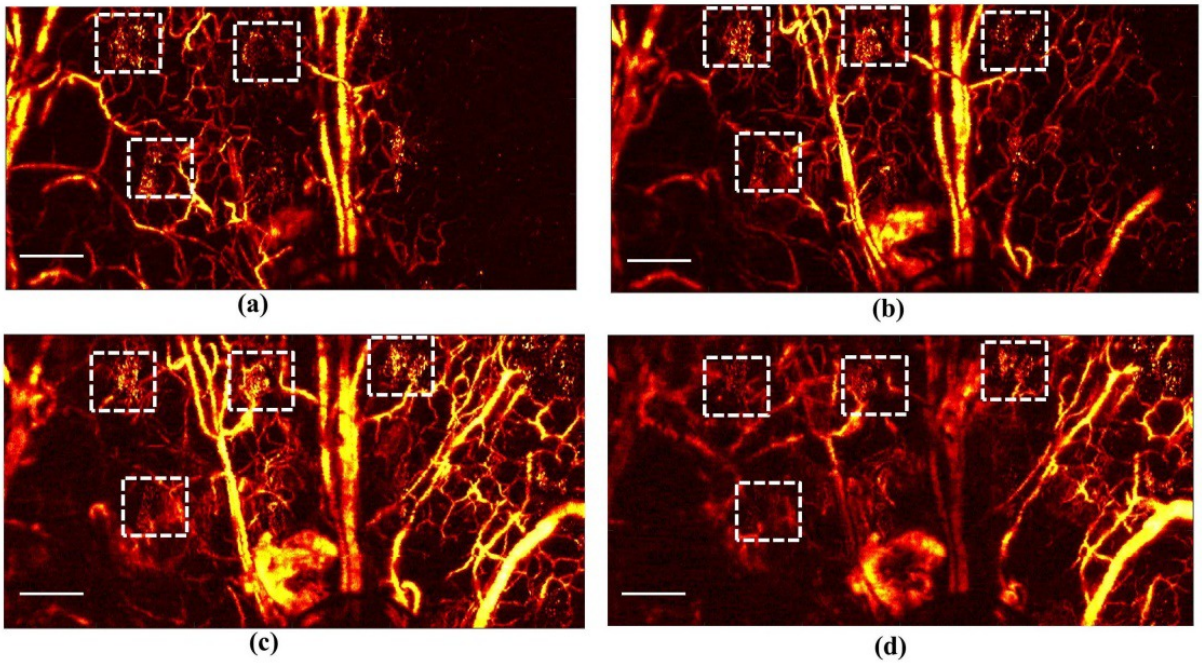

Fig 4**.** *In vivo* photoacoustic image of mouse ear; Maximum amplitude projection images at (a) 0-30 µm (b) 31-60 µm (c) 61-90 µm (d) 91-120 µm from the skin surface after gold coated microneedles insertion. Scale bar corresponds to 300 µm.

From the MAP images in Fig. 4 we could clearly visualize the delivery of nanoparticles. The AUNPs were delivered in the surface as well as 120 μm down the surface.

Conclusions

Here we reported the use of OR-PAM to study the MNs skin penetration and AuNPs delivery on *in vivo* model. We can see that MNs were able to efficiently penetrate skin tissue and deliver the AuNPs up to a depth of ~120 μm. This work reveals the potential use of photoacoustic microscopy in the *in vivo* monitoring of transdermal drug delivery using MNs platforms.

Acknowledgements

The authors would also like to acknowledge the financial support from Tier 2 grant funded by the Singapore Ministry of Education Tier-2 Academic Research Funds (ARC2/15: M4020238 to M.P.), Singapore Ministry of Education Tier-1 Academic Research Funds (RG 131/15 to C.J.X.), NTU-Northwestern Institute for Nanomedicine (M4081502.F40 to C.J.X.). Authors have no relevant financial interests in the manuscript and no other potential conflicts of interest to disclose.

REFERENCES

[1] S. P. Sullivan, N. Murthy, and M. R. Prausnitz, "Minimally Invasive Protein Delivery with Rapidly Dissolving Polymer Microneedles," Advanced Materials, 20(5), 933-938 (2008).

[2] M. Kim, B. Jung, and J. H. Park, "Hydrogel swelling as a trigger to release biodegradable polymer microneedles in skin," Biomaterials, 33(2), 668-78 (2012).

[3] W. Sun, Z. Araci, M. Inayathullah *et al.*, "Polyvinylpyrrolidone microneedles enable delivery of intact proteins for diagnostic and therapeutic applications," Acta Biomater, 9(8), 7767-74 (2013).

[4] K. van der Maaden, W. Jiskoot, and J. Bouwstra, "Microneedle technologies for (trans)dermal drug and vaccine delivery," Journal of Controlled Release, 161(2), 645-55 (2012).

[5] S. Indermun, R. Luttge, Y. E. Choonara *et al.*, "Current advances in the fabrication of microneedles for transdermal delivery," J Control Release, 185, 130-8 (2014).

[6] Y. K. Demir, Z. Akan, and O. Kerimoglu, "Characterization of Polymeric Microneedle Arrays for Transdermal Drug Delivery," PLoS ONE, 8(10), e77289 (2013).

[7] R. L. Siegel, K. D. Miller, and A. Jemal, "Cancer statistics, 2016," CA Cancer J Clin, 66(1), 7-30 (2016).

[8] M. Triesscheijn, P. Baas, J. H. M. Schellens *et al.*, "Photodynamic Therapy in Oncology," The Oncologist, 11(9), 1034-1044 (2006).

[9] I. F. Tannock, "Tumor physiology and drug resistance," Cancer Metastasis Rev, 20(1-2), 123-32 (2001).

[10] P. Vaupel, F. Kallinowski, and P. Okunieff, "Blood flow, oxygen and nutrient supply, and metabolic microenvironment of human tumors: a review," Cancer Res, 49(23), 6449-65 (1989).

[11] R. Arvizo, R. Bhattacharya, and P. Mukherjee, "Gold nanoparticles: Opportunities and Challenges in Nanomedicine," Expert opinion on drug delivery, 7(6), 753-763 (2010).

[12] D. C. Hone, P. I. Walker, R. Evans-Gowing *et al.*, "Generation of Cytotoxic Singlet Oxygen via Phthalocyanine-Stabilized Gold Nanoparticles: A Potential Delivery Vehicle for Photodynamic Therapy," Langmuir, 18(8), 2985-2987 (2002).

[13] M. E. Wieder, D. C. Hone, M. J. Cook *et al.*, "Intracellular photodynamic therapy with photosensitizer-nanoparticle conjugates: cancer therapy using a 'Trojan horse'," Photochem Photobiol Sci, 5(8), 727-34 (2006).

[14] L. Poon, W. Zandberg, D. Hsiao *et al.*, "Photothermal Release of Single-Stranded DNA from the Surface of Gold Nanoparticles Through Controlled Denaturating and Au−S Bond Breaking," ACS Nano, 4(11), 6395-6403 (2010).

[15] H. J. Kwon, Y. Byeon, H. N. Jeon *et al.*, "Gold cluster-labeled thermosensitive liposmes enhance triggered drug release in the tumor microenvironment by a photothermal effect," J Control Release, 216, 132-9 (2015).
[16] M. C. Kearney, S. Brown, M. T. McCrudden *et al.*, "Potential of microneedles in enhancing delivery of photosensitising agents for photodynamic therapy," Photodiagnosis Photodyn Ther, 11(4), 459-66 (2014).
[17] J. G. Fujimoto, "Optical coherence tomography for ultrahigh resolution in vivo imaging," Nat Biotechnol, 21(11), 1361-7 (2003).
[18] R. F. Donnelly, M. J. Garland, D. I. Morrow *et al.*, "Optical coherence tomography is a valuable tool in the study of the effects of microneedle geometry on skin penetration characteristics and in-skin dissolution," Journal of Controlled Release, 147(3), 333-41 (2010).
[19] J. Enfield, M. L. O'Connell, K. Lawlor *et al.*, "In-vivo dynamic characterization of microneedle skin penetration using optical coherence tomography," Journal of Biomedical Optics, 15(4), 046001 (2010).
[20] R. Liu, M. Zhang, and C. Jin, "In vivo and in situ imaging of controlled-release dissolving silk microneedles into the skin by optical coherence tomography," Journal of Biophotonics, 10, 870-877 (2016).
[21] P. K. Upputuri, Z.-B. Wen, Z. Wu *et al.*, "Super-resolution photoacoustic microscopy using photonic nanojets: a simulation study," Journal of Biomedical Optics, 19(11), 116003 (2014).
[22] S. Hu, S. Oladipupo, J. Yao *et al.*, "Optical-resolution photoacoustic microscopy of angiogenesis in a transgenic mouse model." 7564, 756406.
[23] V. Ntziachristos, "Going deeper than microscopy: the optical imaging frontier in biology," Nature Methods, 7(8), 603-14 (2010).
[24] S. Hu, K. Maslov, and L. V. Wang, "Second-generation optical-resolution photoacoustic microscopy with improved sensitivity and speed," Optics Letters, 36(7), 1134-36 (2011).
[25] H. F. Zhang, K. Maslov, G. Stoica *et al.*, "Functional photoacoustic microscopy for high-resolution and noninvasive in vivo imaging," Nature Biotechnology, 24(7), 848-51 (2006).
[26] M. Moothanchery, and M. Pramanik, "Performance Characterization of a Switchable Acoustic Resolution and Optical Resolution Photoacoustic Microscopy System," Sensors, 17(2), 357 (2017).
[27] R. Bi, G. Balasundaram, S. Jeon *et al.*, "Photoacoustic microscopy for evaluating combretastatin A4 phosphate induced vascular disruption in orthotopic glioma," Journal of Biophotonics (2018), published.
[28] M. Moothanchery, A. Sharma, and M. Pramanik, "Switchable Acoustic and Optical Resolution Photoacoustic Microscopy for in vivo small-animal blood vasculature imaging," Journal of Visualized Experiments(124), e55810 (2017).
[29] M. Moothanchery, R. Z. Seeni, C. Xu *et al.*, "In vivo studies of transdermal nanoparticle delivery with microneedles using photoacoustic microscopy," Biomedical Optics Express, 8(12), 5483-5492 (2017).
[30] M. Moothanchery, V. Bavigadda, M. Pramanik *et al.*, "Application of Phase Shifting Electronic Speckle Pattern Interferometry in Studies of Photoinduced Shrinkage of Photopolymer layers," Optics Express, 25(9), 9647-9653 (2017).
[31] M. Moothanchery, I. Naydenova, and V. Toal, "Studies of shrinkage as a result of holographic recording in acrylamide-based photopolymer film," Applied Physics A, 104(3), 899-902 (2011).
[32] K. Park, J. Y. Kim, C. Lee *et al.*, "Handheld Photoacoustic Microscopy Probe," Scientific Reports, 7(1), 13359 (2017).
[33] M. Moothanchery, R. Bi, J. Y. Kim *et al.*, "Optical Resolution Photoacoustic Microscopy Based on Multimode Fibers," Biomedical Optics Express, (2018) (accepted).